# **Inorganic Chemistry**

pubs.acs.org/IC Article

# Augmentation of NIR Circularly Polarized Luminescence Activity in Shibasaki-Type Lanthanide Complexes Supported by the Spirane Sphenol

David Schnable and Gaël Ung\*



Cite This: Inorg. Chem. 2024, 63, 7378-7385



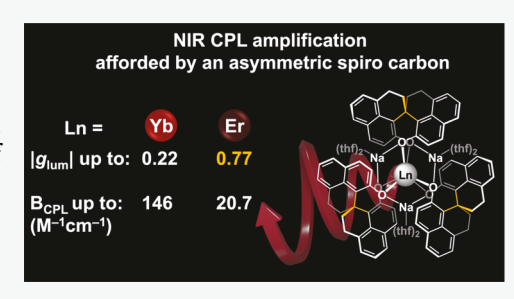
**ACCESS** I

III Metrics & More

Article Recommendations

Supporting Information

**ABSTRACT:** We report two new circularly polarized luminescence (CPL)-active lanthanide complexes emissive in the near-infrared (NIR) region; using sphenol as a supporting ligand, we provide the first reported example of an NIR-emissive lanthanide complex supported by a chiral spirane. Inclusion of a quaternary carbon to impart axial chirality results in dramatic augmentation of the CPL strength of the resultant sphenolate complexes  $(g_{lum} \leq 0.77 \text{ for } [(\text{sphenol})_3\text{ErNa}_3(\text{thf})_6])$  compared to that of their contemporary biaryl-based axially chiral analogues  $(g_{lum} \leq 0.47 \text{ for } [(\text{binol})_3\text{ErNa}_3(\text{thf})_6])$ . Despite similar structural parameters, the rigid spiro carbon of sphenol enables the strongest dissymmetry factors observed to date from Shibasaki-type complexes for both Yb and Er. We also demonstrate the



sensitivity of the reported chiroptical measurements to small variations in instrumental parameters, such as bandpass, and suggest a standardized method or at least that additional detail should be included in future reports to allow for direct comparisons between newly published CPL emitters.

### ■ INTRODUCTION

The efficient generation of circularly polarized (CP) light has been of considerable interest of late, and its application has already provided advances in the fields of spintronic devices, 1,2 enhanced security inks,3 circularly polarized luminescence (CPL) microscopy<sup>4</sup> and in the production of a new generation of 3-dimensional displays. Conversion of traditional light sources into circularly polarized light is energy-inefficient; for broad-scale application, the development of faster detection methods<sup>6</sup> and better means of direct emission, through circularly polarized luminescence (CPL), are both areas of intense interest. 7-11 Regarding the latter, due to their favorable photophysical properties, emissive members of the lanthanide series have so far been the most successful at the efficient generation of high-purity circularly polarized light. Both the emitters with the strongest overall dissymmetry factor 12 (a measure of CP emission purity, defined as  $2 \times (I_L - I_R)/(I_L +$  $I_{\rm R}$ ) =  $g_{\rm lum}$ )<sup>13</sup> and CPL brightness (a measure of overall CPL intensity, defined as  $1/2 \varepsilon \times \Phi_f \times g_{lum} = B_{CPL})^{14,15}$  are visibly emissive lanthanide complexes.

Recently, new CPL applications in the field of fiber-optic telecommunications have been uncovered. The near-infrared (NIR) region, particularly that centered around 1550 nm, is favorable for this purpose due to the low transmission loss of traditional fiber-optic cables in this region. Development of strong CPL emitters in this region could result in advances in data transmission rates due to the added chiroptical information available. For this purpose, the lanthanide erbium has been targeted due to its very favorable transition type, <sup>17</sup>

even among the lanthanides, and its emission window in the 1450–1650 nm region. Additionally, the development of CPL-active emitters in other parts of the NIR region is also desired due to emerging applications in medical imaging. 4,18–25

Very few examples of CPL-active emitters in the far NIR region (>1200 nm) have been reported. Zinna, Di Bari, and co-workers have previously reported that pyridine-bisoxazoline could generate CPL emission from Er,<sup>26</sup> with good circular polarization but only modest brightness ( $g_{lum} = 0.33$ ,  $B_{CPL} =$ 0.7 M<sup>-1</sup> cm<sup>-1</sup>; although these values are not directly comparable, see below). We also reported two other examples of CPL activity from Er, first from the binolate-supported (Figure 1) erbium-containing Shibasaki complex [(bino-1)<sub>3</sub>ErNa<sub>3</sub>(thf)<sub>6</sub>],<sup>27</sup> which achieved stronger  $B_{CPL}$  and  $g_{lum}$ values of 57.3 M<sup>-1</sup> cm<sup>-1</sup> and 0.47, respectively. The dissymmetry factor of this system could be further improved by slight alteration of the ligand in an attempt to modulate its electric dipole and improve coupling, though at the expense of overall brightness, as shown by the values obtained by the vanol-supported analogue [(vanol)<sub>3</sub>ErNa<sub>3</sub>(thf)<sub>6</sub>] ( $g_{lum} = 0.64$ ,  $B_{\rm CPL} = 19.5 \; {\rm M}^{-1} \; {\rm cm}^{-1}$ , measured in the same conditions as the binol analogue).<sup>28</sup> This trade-off between strong  $g_{lum}$  and

Received: January 30, 2024 Revised: March 26, 2024 Accepted: March 27, 2024 Published: April 5, 2024





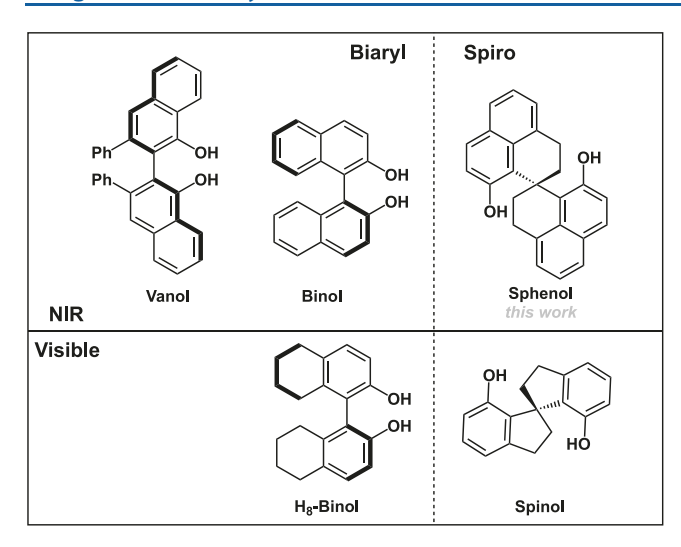


**Figure 1.** Reported axially chiral Shibasaki-type ligands for the generation of CPL-active lanthanide complexes.

diminished brightness has also been observed in the CsEr-(hfbc)<sub>4</sub> system, recently reported by Di Bari and co-workers, which achieves  $g_{\text{lum}} = 0.83$ , the highest reported dissymmetry factor to date in the NIR region, but with a brightness of  $0.017-0.578 \text{ M}^{-1} \text{ cm}^{-1}$ . The low quantum yield of the system is likely due to weak sensitization by the supporting chromophore, presumably due to less-than-ideal placement of the ligand's triplet energy level.

We note that in lanthanides (and likely actinides) as well as chromium,  $^{30,31}$  overlapping CPL signals of opposite signs can often be observed. In those cases, dissymmetry factor values (and thus  $B_{\rm CPL}$ ) significantly depend on experimental setups (as demonstrated below). Due to a lack of experimental transparency in the reports cited above, the values and comparisons discussed above provide valuable insights but must be considered with caution.

Most Shibasaki-type complexes reported to date depend on an axially chiral ligand utilizing a sterically hindered biaryl system to impart chirality, as is the case in both the binol and vanol ligands previously discussed. However, we have previously observed that significant improvement in CPL metrics could be obtained when a ligand whose chirality arises from a rigid spiro carbon. Our group has reported a pair of Shibasaki-type complexes supported by phenolate chromophores, which are more suitable for sensitization of lanthanides emitting in the visible region. First, a reduced H<sub>8</sub>-binolate ligand was used to generate CPL-active complexes achieving a g<sub>lum</sub> value of up to 0.44 for [(H<sub>8</sub>-binol)<sub>3</sub>TbNa<sub>3</sub>(thf)<sub>6</sub>], corresponding to a  $B_{CPL}$  of 782 M<sup>-1</sup> cm<sup>-1,32</sup> In an effort to further improve these metrics, we subsequently reported analogues supported by spinol, a chiral spirane.<sup>33</sup> This modification resulted in an augmentation of the glum values of the analogous complex [(spinol)<sub>3</sub>TbNa<sub>3</sub>(thf)<sub>6</sub>] to 0.53, presumably due to the increased rigidity provided by the conformationally locked quaternary carbon. Due to a drastically increased quantum yield resulting from more favorable sensitization energetics, the  $B_{CPL}$  value also increased to 3,760 M<sup>-1</sup> cm<sup>-1</sup>, making this compound the brightest CPL emitters of any type reported to date.

To further improve the CPL metrics attainable in the NIR region, we sought to generate NIR-emissive lanthanide complexes supported by a chiral spirane to determine if

further CPL augmentation can be obtained, as in the case of H<sub>8</sub>-binol/spinol. Sphenol, a spinol-analogue containing a naphthol chromophore, has been previously reported for use in asymmetric catalysis.<sup>34</sup> No coordination chemistry has been reported for sphenol with any metals, but we hypothesized that its similarity to both binol and spinol may allow generation of these complexes by similar methods. We thus selected sphenol as a candidate for investigation to determine if coordination with the lanthanides is possible and if further improvement of the CPL metrics in these systems can be achieved.

# ■ RESULTS AND DISCUSSION

**Synthesis and Complex Characterization.** Synthesis of the sphenol ligand has been reported previously;<sup>34</sup> in our hands, yields were considerably lower than reported and minor modifications were made to compensate. Full experimental details for the ligand synthesis are provided in the Supporting Information.

With the ligand in hand, we assessed the possibility for the generation of a Shibasaki-type complex in coordination with the lanthanides. To clarify interpretation of nuclear magnetic resonance (NMR) spectra, first attempts were made using the trivalent, diamagnetic metal yttrium, a similarly sized analogue for the later lanthanides, as the target NIR-emissive lanthanides are paramagnetic. Reacting three equivalents of the ligand in tetrahydrofuran solution with a mixture of one equivalent of YCl<sub>3</sub> and six equivalents of the base sodium hexamethyldisilazide (NaHMDS) for 4 h at room temperature (Scheme 1)

Scheme 1. Synthesis of tris- Homoleptic Sphenol-Supported Lanthanide Complexes, [((S)-Sphenol)<sub>3</sub>LnNa<sub>3</sub>(thf)<sub>6</sub>], Ln = Y, Er, Yb<sup>a</sup>

<sup>a</sup>The synthesis of the enantiomeric complexes was conducted identically.

resulted in a turbid solution due to the precipitation of the sodium chloride byproduct. Filtering this suspension allowed for isolation of the tris-homoleptic lanthanide complex  $[(sphenol)_3YNa_3(thf)_6]$  as a white solid after removal of the volatiles under reduced pressure.

NMR spectra of this complex collected from  $d_3$ -acetonitrile solutions (Figure 2) show only a single set of ligand resonances, indicating expected  $D_3$  symmetry. The loss of the broad singlet visible in the free ligand spectrum at ca. 6.0 ppm was indicative of successful deprotonation of the ligand by NaHMDS *in situ*. Minor shifting of the ligand peaks occurs on complexation and is highlighted in Figure 2. In all cases, broad resonances from a minor species of similar symmetry were also present, visible in Figure 2 as small peaks at 6.45 and 7.45 ppm. These are discussed in more detail in later sections and in the Supporting Information.

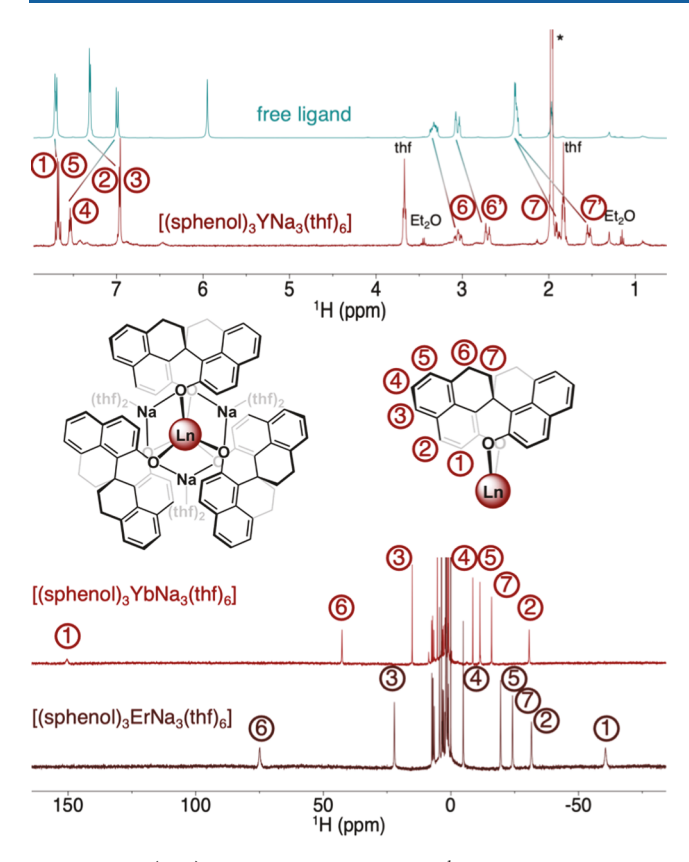


**Figure 2.** (top) Comparison of the  $^{1}$ H NMR spectra of [(sphenol)<sub>3</sub>YNa<sub>3</sub>(thf)<sub>6</sub>] before and after complexation, collected from solutions in  $d_3$ -acetonitrile. See also Figures S1–S6. (center) Map of proton resonances for assignment. (bottom)  $^{1}$ H NMR spectra of the paramagnetic, emissive lanthanide complexes, collected from solutions in  $d_3$ -acetonitrile. Resonances arising from the paramagnetic complexes are marked. See also Figures S1–S6. Proton assignments for each resonance are discussed in more detail both later in this paper and in the SI.

The same method was used to synthesize the emissive analogues, starting from the appropriate lanthanide trichloride salt. While paramagnetically shifted, the obtained  $^1\mathrm{H}$  NMR spectra (Figure 2) each have at most seven peaks present, indicating that the  $D_3$  symmetry is conserved despite the slight change in metal size. Identically to the yttrium complex, small diamagnetic impurities resembling the free ligand are present in the 6–8 ppm region.

**Luminescence and Chiroptical Properties.** With the complexes in hand, we were able to characterize their chiroptical properties. The absorbance spectra of both complexes (Figures S8 and S9) display only the expected absorbance in the ultraviolet (UV) region consistent with the  $\pi \to \pi^*$  transition internal to the ligand's chromophore. The [(sphenol)<sub>3</sub>YbNa<sub>3</sub>(thf)<sub>6</sub>] complexes were found to be CD-active on this absorption transition with  $|g_{abs}| \le 2.2 \times 10^{-3}$ . The spectra were found to be mirror images, as expected for a pair of enantiomeric complexes (Figure 3).

The [(sphenol)<sub>3</sub>YbNa<sub>3</sub>(thf)<sub>6</sub>] complexes are luminescent on excitation at 365 nm and display the typical sharp emission profile for an Yb emitter, with an emission maximum at 973 nm in the NIR region. The quantum yield of the complex was recorded by comparison to previously reported [(bino-l)<sub>3</sub>YbNa<sub>3</sub>(thf)<sub>6</sub>] ( $\Phi_f = 0.17$  in tetrahydrofuran)<sup>23</sup> and measured as weaker at 0.075 under identical conditions.

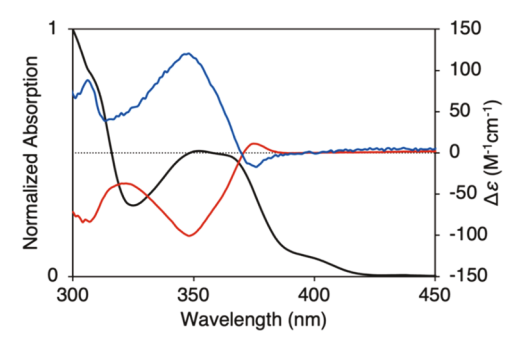
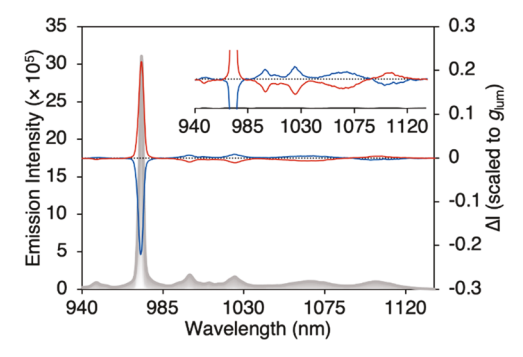


Figure 3. Circular dichroism spectra of  $[(sphenol)_3YbNa_3(thf)_6]$ , collected from  $4.3 \times 10^{-5}$  M solutions in tetrahydrofuran.  $[((R)-sphenol)_3YbNa_3(thf)_6]$  is traced in red, and its enantiomer is traced in blue. Absorption spectrum presented as a black trace in the background. Bandpass: 1.0 nm. See also Figure S22 for the analogous plot for  $[(sphenol)_3ErNa_3(thf)_6]$ .

Lifetime measurements were also performed and are discussed in later sections. More details regarding these photophysical measurements are available in the Supporting Information.

Circularly polarized luminescence spectra were collected from 10<sup>-4</sup> M solutions of the [(sphenol)<sub>3</sub>YbNa<sub>3</sub>(thf)<sub>6</sub>] complexes in THF (Figure 4) on excitation by a fixed



**Figure 4.**  $\Delta I$   $(I_L - I_R)$  CPL plot normalized to  $g_{lum}$  for [(sphenol)<sub>3</sub>YbNa<sub>3</sub>(thf)<sub>6</sub>], collected from  $2.3 \times 10^{-4}$  M solutions in tetrahydrofuran. The CPL spectrum of [((R)-sphenol)<sub>3</sub>YbNa<sub>3</sub>(thf)<sub>6</sub>] is traced in red, and its enantiomer is traced in blue. Inset with a plot at  $20 \times$  magnification. Total emission traced in gray in the background. See Figures S15–S17 for additional CPL plots. Excitation at 380 nm, bandpass 1.0 nm.

wavelength 380 nm LED. The dissymmetry factors at 972 nm (the 0'  $\rightarrow$  0 transition) were recorded at  $|g_{lum}| \leq 0.22$ , slightly stronger than both  $[(vanol)_3YbNa_3(thf)_6]$   $(|g_{lum}| \le 0.21)$  and  $[(binol)_3 YbNa_3(thf)_6]$  ( $|g_{lum}| \leq 0.17$ ). These measurements were done under identical experimental conditions, allowing for direct comparisons. The lower energy, less emissive Stark levels were also found to be CPL-active with comparable magnitude of  $|g_{lum}| \le 0.14$ , peaking at 1065 nm. Weak CPL activity was observed for the higher energy stark level with I  $g_{\text{lum}} \leq 0.05$  at 950 nm. The overall shape of the CPL spectrum generally mimics that of [(vanol)<sub>3</sub>YbNa<sub>3</sub>(thf)<sub>6</sub>], having a trisignate shape at wavelengths less than 1065 nm. The vanol spectrum (Figure S24) does feature an additional sign inversion on the Stark level centered at 1080 nm, which is not present in the spectra from [(sphenol)<sub>3</sub>YbNa<sub>3</sub>(thf)<sub>6</sub>], likely due to overlap of adjacent levels due to the significant shifting of the later stark levels, which can be ascribed to changes in the crystal field splitting. The quantum yield and dissymmetry factor, together with the measured extinction coefficient of

Table 1. Tabulated CPL Brightness Metrics for All Published NIR-Emissive Shibasaki-Type Analogues

Ln complex	$\Lambda$ (nm)	$\varepsilon~(\mathrm{M}^{-1}~\mathrm{cm}^{-1})$	$\Phi_{ ext{F}}$	$g_{ m lum}$	$B_{\rm CPL}~({ m M}^{-1}~{ m cm}^{-1})$	$^{\rm Ln}B_{\rm CPL}^{29}~({\rm M}^{-1}~{\rm cm}^{-1})$
$[(sphenol)_3ErNa_3(thf)_6]^b$	1540	19,060	0.0028	0.77	20.7	16.5
$[(vanol)_3ErNa_3(thf)_6]^{28,b}$	1540	12,900	0.0048	0.64	19.5	11.5
$[(binol)_3ErNa_3(thf)_6]^{27,b}$	1540	42,000	0.0058	0.47	57.3	22.1
$[(binol)_3Er(TMGH)_3]^{29}$	1545	59,279	$2 \times 10^{-6}$	0.29	0.017	<u>_</u> a
$[(sphenol)_3YbNa_3(thf)_6]^b$	973	17,820	0.075	0.22	146.3	66.0
$[(\text{vanol})_3\text{YbNa}_3(\text{thf})_6]^{28,b}$	975	11,500	0.101	0.21	122.3	38.8
$[(binol)_3 Yb Na_3 (thf)_6]^{27,b}$	975	26,000	0.17	0.17	379	160.0
$[(binol)_3Yb(TMGH)_3]^{29}$	954	<u>_</u> a	_a	0.066	<u>-</u> a	<u>_a</u>

<sup>a</sup>To our knowledge, these data have not been published, and thus, these metrics are not available for comparison. <sup>b</sup>These bolded values were collected under identical experimental conditions and, therefore, are directly comparable to one another.

17,820  $M^{-1}$  cm<sup>-1</sup>, equate to a  $B_{\rm CPL}$  value of 146.3  $M^{-1}$  cm<sup>-1</sup>. We have recently proposed an alternate method of calculating  $B_{\rm CPL}$ , which accounts for closely spaced peaks of opposite CPL sign within the same transition, <sup>29</sup> and according to this formula, the  $B_{\rm CPL}$  value is reduced to 66.0  $M^{-1}$  cm<sup>-1</sup> (See Table 1).

The two highest reported  $g_{lum}$  values for Yb emitters to date are  $(TMA)(H_3O)[Yb_2(S-BTHP)_4]$   $(|g_{lum}| \le 0.81)^{31}$  and  $CsYb(hfbc)_4$   $(|g_{lum}| \le 0.38)^{.11,25}$  To date, our group has also published two CPL-active Yb complexes with  $g_{\text{lum}}$  varying from 0.17 to 0.21 and  $B_{\text{CPL}}$  from 122.3 to 379  $\text{M}^{-1}$  cm<sup>-1</sup>; of our three  $D_3$  symmetrical examples, sphenol displays slightly stronger circular polarization strength but remains limited in brightness due to its diminished molar absorptivity and quantum yield. Possibly due to symmetry considerations, the D<sub>3</sub> symmetrical Yb Shibasaki complexes have yet to approach the CPL magnitude of the C4 examples CsYb(hfbc)4 and (TMA)(H<sub>3</sub>O)[Yb<sub>2</sub>(S-BTHP)<sub>4</sub>]. Despite this, all of these Yb emitters are well placed within the optical transparency window of tissue and therefore may enable the design of derivatives for use as optical probes in vivo. The emission profile of Yb is less suitable, however, for use in fiber-optic telecommunications, another desirable application for NIR CPL, for which CPL-active Er complexes are preferred.

The [(sphenol) $_3$ ErNa $_3$ (thf) $_6$ ] complexes were also found to be luminescent on excitation at 380 nm, displaying the typical emission spectrum of Er in the NIR region, much deeper into the region with an emission maximum at 1545 nm. Quantum yield measurements were recorded for [(spheno-l) $_3$ ErNa $_3$ (thf) $_6$ ] from dilute solutions in tetrahydrofuran, comparing against the reference [(binol) $_3$ ErNa $_3$ (thf) $_6$ ] ( $\Phi_F$  = 0.0058 in tetrahydrofuran) $^{23}$  and, like the Yb sphenolate analogue, were found to be slightly weaker at 0.0028. The weaker relative emission strength in both cases is likely due to increased vibrational quenching from additional C–H bonds present in the saturated ligand backbone as compared to unsaturated binol.

Circularly polarized luminescence spectra were collected from  $10^{-4}$  M solutions of the  $[(sphenol)_3ErNa_3(thf)_6]$  complexes in THF (Figure 5) on excitation by a fixed wavelength 380 nm LED. As previously observed with  $[(vanol)_3ErNa_3(thf)_6]$ , the higher energy stark level centered at 1460 nm demonstrated no significant CPL activity. However, the adjacent levels at 1545 and 1570 nm showed strong CPL activity of the opposite sign; the former (the  $0' \rightarrow 0$  transition) measuring  $|g_{lum}| \leq 0.77$  and the latter  $\leq 0.35$ . The Er analogue was found to have an extinction coefficient of 19,060 M<sup>-1</sup> cm<sup>-1</sup>, affording an overall  $B_{CPL}$  of 20.7 M<sup>-1</sup>cm<sup>-1</sup> (see also Table 1). Our obtained  $B_{CPL}$  value is marginally

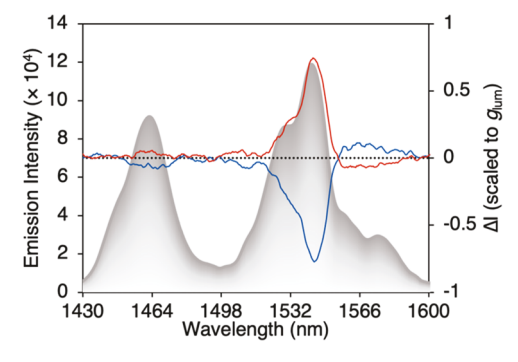


**Figure 5.**  $\Delta I$   $(I_{\rm L}-I_{\rm R})$  CPL plot normalized to  $g_{\rm lum}$  for [(sphenol) $_3$ ErNa $_3$ (thf) $_6$ ], collected from  $1.5\times 10^{-4}$  M solutions in tetrahydrofuran. The CPL spectrum of [((R)-sphenol) $_3$ ErNa $_3$ (thf) $_6$ ] is traced in red, and its enantiomer is traced in blue. Total emission traced in gray in the background. See Figures S18 and S20 for additional CPL plots. Excitation at 380 nm, bandpass 10 nm.

higher than that of  $[(vanol)_3 Er Na_3(thf)_6]$  (19.5 M<sup>-1</sup> cm<sup>-1</sup>), as well as the non-Shibasaki-type Er complexes supported by pyridine-bisoxazoline (0.7 M<sup>-1</sup> cm<sup>-1</sup>) and CsEr(hfbc)<sub>4</sub> (0.58 M<sup>-1</sup>cm<sup>-1</sup>). Despite the significantly increased  $g_{lum}$  value,  $[(sphenol)_3 Er Na_3(thf)_6]$  has a lower extinction coefficient and quantum efficiency than those of the previously reported binolate analogues, resulting in a lower overall  $B_{CPL}$  value (57.3 M<sup>-1</sup> cm<sup>-1</sup> for  $[(binol)_3 Er Na_3(thf)_6]$ ). A similar trade-off is also observed in our prior work on  $[(vanol)_3 Er Na_3(thf)_6]$ . Further synthetic efforts to optimize both  $g_{lum}$  and  $B_{CPL}$  simultaneously are still required to maximize all metrics to increase practical usability. For the sphenol system, by our previously proposed alternate method of  $B_{CPL}$  calculation, we instead find a  $^{Ln}B_{CPL}$  value of 16.5 M<sup>-1</sup>cm<sup>-1</sup> (see also Table 1).

The emission strength afforded by  $[(sphenol)_3ErNa_3(thf)_6]$ modest quantum yield allowed for collection of the spectrum with a bandpass of 10 nm; this turned out to be advantageous, as an increase to a bandpass of 26 nm results in blending of the opposite signals and a measurable |glum| value of only 0.65 and 0.25, at 1545 and 1570 nm, respectively. Subsequently, the  $B_{\rm CPL}$  values of the complex were reduced to 17.3 M<sup>-1</sup> cm<sup>-1</sup> and, by our alternate method, 13.7 M<sup>-1</sup> cm<sup>-1</sup>. We have observed that even slight changes to the experimental setup, such as altered bandpass, can have significant impacts on the emission line widths and CPL intensity, likely due to blending of neighboring Stark levels of an opposite CPL sign. This implies that any meaningful direct comparisons between systems will require a detailed disclosure of the experimental setup. The comparison of values from other groups, akin to those made in our manuscripts and others, 15,29,35,36 can provide a general trend but must be interpreted with caution.

We have endeavored to include as much information about the experimental setup as possible in Supporting Information for this work and have included footnotes on all values in Table 1, which is directly comparable, owing to their identical collection conditions. We suggest that, to enable direct comparisons between complexes in the future, an equivalent experimental setup be used, or at the least that an equivalent level of experimental detail accompanies future publications of CPL-active complexes.

Computational Structural Analysis. To help explain the strong CPL activity, we sought to measure structural parameters to compare them to other similar complexes. Unfortunately, confirmation that these complexes are isostructural in the solid state could not be obtained through X-ray diffraction (XRD), as in the present case, suitable quality crystals were not able to be grown. The high symmetry of the NMR spectra acquired from the complexes indicates that they retain the expected  $D_3$  symmetry in solution, as observed in other Shibasaki-type lanthanide complexes; this, in addition to the high degree of similarity between the emission and chiroptical spectra of the [(sphenol)<sub>3</sub>LnNa<sub>3</sub>(thf)<sub>6</sub>] complexes and their vanol and binol analogues (see Figure S24), indicates they likely have similar solution-state structures. This was also the case in our previously reported spirane-supported complexes [(spinol)<sub>3</sub>LnNa<sub>3</sub>(thf)<sub>6</sub>], which are structurally similar to those of [(H<sub>8</sub>-binol)<sub>3</sub>LnNa<sub>3</sub>(thf)<sub>6</sub>] in the solid state and have nearly identical emission patterns in solution. The [(sphenol)<sub>3</sub>LnNa<sub>3</sub>(thf)<sub>6</sub>] stoichiometry was also further corroborated by using elemental analysis.

As an alternative to XRD, to assess the ligand configuration about the lanthanide center, an optimized coordination geometry was computed for [(sphenol)<sub>3</sub>LuNa<sub>3</sub>(thf)<sub>6</sub>] by using density functional theory (DFT) methods and the ORCA 5.0.4 software suite. Lutetium was chosen due to its trivalent cation being closed-shell, as open-shell species are known to cause significant challenges for SCF convergence<sup>37</sup> while retaining a similar size to the CPL-active erbium and ytterbium centers. The B3LYP functional, further augmented by Grimme's D3 dispersion corrections and Becke-Johnson damping, 38,39 was used alongside ZORA relativistic methods. 40,41 Lutetium, sodium, and the chelating oxygen atoms were all treated using Ahlrich's triple-ζ def2-tzvp basis set augmented with polarization, while the remainder of the ligand backbone employed the double-\( \zeta\) def2-svp basis set. 42 The calculation also included the solution-phase solvation model CPCM to compensate for solvent effects from solvating tetrahydrofuran. 43 Similar methods have been used previously to estimate the solution-state structures of NIR-emissive lanthanide complexes.<sup>26</sup> After geometry optimization, the output structure was subjected to single-point vibrational analysis to confirm the absence of residual imaginary vibrational modes, indicating that the output had reached a minimum on the potential energy surface. For more details on the computational methods, see the Supporting Information (Figure S25, Tables S5 and S6).

To confirm that the computed [(sphenol)<sub>3</sub>LuNa<sub>3</sub>(thf)<sub>6</sub>] structure was a suitable stand-in for the CPL-active paramagnetic analogues, we first sought to correlate the computed experimental properties with those measured from the Yb and Er analogues. The presence of a paramagnetic metal center in organolanthanide complexes typically causes extreme shifting and broadening of NMR resonances, which confounds interpretation of their NMR spectra; however, some

techniques are available to glean more solution-state structural information through NMR. When in proximity to a paramagnetic center, strong spin-electron paramagnetic interactions become the dominant means of magnetic relaxation and usually result in drastically decreased  $T_1$  relaxation times for protons relatively close to the metal center. The degree of  $T_1$  shortening is known to be highly distance sensitive and proportional to  $1/r^6$ , with r being the distance from the unpaired electron to the observed nucleus. Brachais and coworkers have exploited comparisons between relative M—H distances obtained from  $T_1$  relaxation studies and those measured from solid-state crystal structures to assign resonances in the NMR spectrum.

In the absence of solid-state data, we instead compared the distances calculated from our geometry-optimized structure to those estimated from  $T_1$  relaxation times and found they were in reasonable agreement (average %error 5.5% for Yb and 11.0% for Er), despite the slight change to the metal size (see Figure S7). Using this information, we were able to provide assignments for all of the <sup>1</sup>H NMR resonances shown in Figure 2. For most resonances, on changing from Yb to the more paramagnetic Er, the degree of paramagnetic shifting roughly doubles in magnitude, which is consistent with their relative magnetic moments (as calculated by Hund and Van Vleck, 4.50 and 9.60 for Yb and Er, respectively). 46,47 The exception to this trend is resonance 1, which by the process of elimination can be assigned to the proton ortho to the chelating oxygen, which displays both unexpectedly small shifting intensity as well as inversion of the shift direction on changing the central metal from Yb to Er (+148 and -71 ppm)respectively). Similar effects have previously been observed by Parker and co-workers, in which breakdown of the traditional distance dependence in  $T_1$  values occurs for protons in very close proximity to metals displaying uniaxial magnetic anisotropy (such as Er and Yb).48

Given the reasonable  $DFT/T_1$  distance correlation, indication of the expected D<sub>3</sub> symmetry by <sup>1</sup>H NMR, confirmation of [(sphenol)<sub>3</sub>LnNa<sub>3</sub>(thf)<sub>6</sub>] stoichiometry by EA, and similar experimental properties to the prior published Shibasaki-type complexes, we posit that our DFT geometryoptimized Lu structure is a suitable point of comparison between the sphenolate complexes and other Shibasaki-type complexes. Looking more closely at the optimized sphenol structure, despite the small change in the size of the central metal, the optimized sphenol structure (Figure 6) was found to be largely similar to the previously reported [(bino-1)<sub>3</sub>YbNa<sub>3</sub>(thf)<sub>6</sub>] and [(vanol)<sub>3</sub>YbNa<sub>3</sub>(thf)<sub>6</sub>] complexes. The only exception is that [(sphenol)<sub>3</sub>LuNa<sub>3</sub>(thf)<sub>6</sub>] has a significantly larger torsion angle between the two planes of the naphthol chromophores (~97°), unlike the biaryl variants in which this angle can compress to 63-65° through rotation around the sterically hindered single bond. In the case of sphenol, this effect can be ascribed to the increased ligand rigidity provided by the conformationally locked spiro carbon, from which the axial chirality of sphenol arises.

This increased rigidity is also likely the source of the augmented  $g_{lum}$  relative to that of the binolate complexes despite their otherwise similar distortion parameters (see Table S2). We have previously observed the same effect when comparing complexes derived from the axially chiral biaryl ligand  $H_8$ -binol ([( $H_8$ -binol) $_3$ TbNa $_3$ (thf) $_6$ ],  $g_{lum}$  up to 0.32) to those supported by their spirane analogue spinol ([(spi-

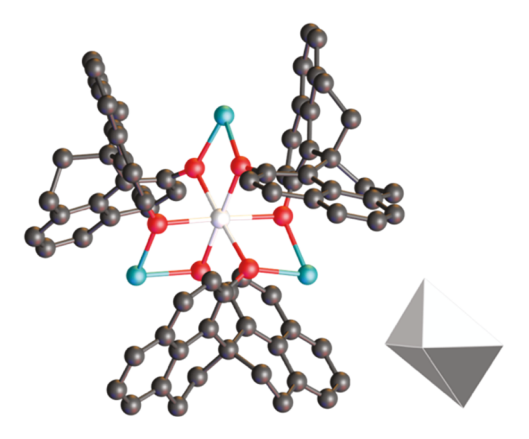


**Figure 6.** Top-down view of the DFT-optimized structure of [(sphenol)<sub>3</sub>LuNa<sub>3</sub>(thf)<sub>6</sub>]. Sodium-bound tetrahydrofuran molecules and hydrogen atoms have been omitted for clarity. An equatorial view of the distorted-octahedral Lutetium coordination polyhedron is shown on the right. See also **Figure S23**. Computational inputs and tables of output coordinates can be found in the SI as Tables S3 and S4.

nol) $_3$ TbNa $_3$ (thf) $_6$ ],  $g_{lum}$  up to 0.53), both of which have been used to generate CPL in the visible region.  $^{32,33}$ 

**Ligand Stability.** During the synthesis of the complexes, we noted that the reaction yields varied significantly between batches, particularly in cases where the reaction time was elongated or when the reaction was not protected from light. During photoirradiation of a sample for 20 h, the lanthanide luminescence intensity slowly diminished and the solutions were noted to take on a blueish hue over time, visible in the absorbance spectrum as the rise of an absorbance peak at ca. 630 nm (see Figures S10 and S11). This decomposition product is also the source of the minor extraneous NMR peaks previously mentioned and visible in Figure 2 (see also Figure S12). This decomposition may also account for the difficulty in growing single crystals of this complex. All efforts to identify the decomposition product failed, but additional experimental data is available in the Supporting Information.

Likely due to this presumed in situ decomposition of the ligand, the luminescence lifetimes of both [(spheno-1)<sub>3</sub>ErNa<sub>3</sub>(thf)<sub>6</sub>] and [(sphenol)<sub>3</sub>YbNa<sub>3</sub>(thf)<sub>6</sub>] do not fit well to a monoexponential decay pattern, indicating there is likely more than one species present in solution (Figures S13 and S14).<sup>49</sup> Luminescence decay data was collected from dilute solutions in tetrahydrofuran at room temperature with concentrations of  $1.1 \times 10^{-5}$  M for [(sphenol)<sub>3</sub>ErNa<sub>3</sub>(thf)<sub>6</sub>] and  $3.1 \times 10^{-6}$  M for [(sphenol)<sub>3</sub>YbNa<sub>3</sub>(thf)<sub>6</sub>]. The concentration for the former was slightly increased to account for its much weaker luminescence quantum yield. Data from both most closely modeled as two superimposed exponential decay functions, indicating there are at least two species in solution. <sup>50</sup> [(sphenol)<sub>3</sub>YbNa<sub>3</sub>(thf)<sub>6</sub>] displayed emission with lifetimes of 11.6 and 108  $\mu$ s, while [(sphenol)<sub>3</sub>ErNa<sub>3</sub>(thf)<sub>6</sub>] measured at 2.8 and 279  $\mu$ s. The former of each of these values is similar to previously reported complexes of each respective emissive metal, particularly other examples of Shibasaki-type complexes, while the latter are exceptionally long in both cases and may arise from a partially decomposed complex forming in situ.

#### CONCLUSIONS

We have reported the third member of a series of NIR-CPL-active complexes of the form [("di-naphthol")LnNa<sub>3</sub>(THF)<sub>6</sub>], otherwise known as Shibasaki-type complexes. In this instance, we applied sphenol as a supporting ligand to, for the first time, integrate a quaternary spiro carbon for the induction of NIR-CPL activity. As is also the case for our previously reported spinolate complexes for visible CPL, sphenol enables improved CPL strength over all other reported Shibasaki-type complexes emitting in this region, likely due to increased rigidity compared to the more commonly employed sterically hindered biaryl-based ligands.

For practical purposes, erbium is of particular interest for many applications, as its emission window lies in the highly sought-after telecom-C band and increased chiroptical purity can only be beneficial for future utility in telecommunications. The CPL augmentation provided by the inclusion of a chiral spirane ligand is most evident for [(sphenol)<sub>3</sub>ErNa<sub>3</sub>(thf)<sub>6</sub>] (I  $g_{\text{lum}}$  |  $\leq 0.77$ ,  $B_{\text{CPL}} = 20.7 \text{ M}^{-1} \text{ cm}^{-1}$ ) whose  $g_{\text{lum}}$  is among the highest reported in the NIR region to date.

While this ligand platform enables augmented  $g_{lum}$  metrics, its brightness remains limited by modest quantum yields and molar absorptivity metrics. Additionally, we have identified that a low torsion angle between the biaryl moieties was a synthetic design limit, evidenced by the appreciably unstable nature of sphenol under Lewis acidic conditions, including when complexed to a lanthanide metal. Further synthetic work that can maximize  $g_{lum}$ , quantum yield, and molar absorptivity while improving stability should thus be facilitated with that knowledge.

Finally, we have demonstrated high sensitivity of the reported chiroptical measurements to even small variations in instrumental parameters, such as the bandpass. We suggest that in all future publications of CPL-active complexes either the same bandpass is consistently used or at least full experimental disclosure should be included to allow for better comparisons between newly published CPL emitters.

# EXPERIMENTAL SECTION

Materials and Methods. All synthetic manipulations were performed under an anhydrous atmosphere of nitrogen using standard Schlenk techniques unless otherwise stated. Storage and manipulations were performed in a nitrogen-filled glovebox equipped with an atmospheric purification train, in which oxygen and water levels were kept constantly below 2 ppm. Full experimental details for the determination of all photophysical metrics are provided in the Supporting Information.

Sphenol was prepared according to literature methods.<sup>30</sup> Full experimental details are given in the Supporting Information.

**Synthetic Methods.** [((S)-Sphenol)<sub>3</sub>YNa<sub>3</sub>(thf)<sub>6</sub>]—General Procedure. To a 20 mL vial was added 4 mg of YCl<sub>3</sub> (20  $\mu$ mol) as a solid, followed by a magnetic stir bar and 2 mL of tetrahydrofuran (THF), and then the mixture was stirred 10 min to dissolve. To a separate 4 mL vial was added 23 mg NaHMDS (125  $\mu$ mol, 6 equiv), followed by 2 mL THF to dissolve. This solution of base was then added dropwise to the stirring metal salt. An additional 2 mL THF was used to rinse the vial to ensure complete transfer, then the mixture is again stirred for 10 min. The 20 mL vial was then tightly wrapped with aluminum foil to keep its contents under dark. To a separate 4 mL vial was then added 22 mg of (S)-sphenol (62  $\mu$ mol, 3 equiv), followed by 2 mL of THF to dissolve. The ligand solution was added dropwise to the stirring metal salt, and then the resulting reaction mixture was stirred in the dark for 4 h at room temperature. Upon completion, the turbid reaction mixture was filtered through a 2 cm pad of Celite loaded in a pipet to remove the NaCl byproduct, followed by removal of the

volatiles under reduced pressure, to afford 30 mg of the title compound (18  $\mu$ mol, 90%) as a white solid.

<sup>1</sup>H NMR (400 MHz, CD<sub>3</sub>CN) δ 7.68 (q, J = 8.8 Hz, 4H), 7.54 (t, J = 5.3 Hz, 2H), 6.96 (d, J = 5.6 Hz, 4H), 3.12–2.99 (m, 2H), 2.71 (dt, J = 16.4, 3.9 Hz, 2H), 1.94–1.86 (m, 2H), 1.54 (dt, J = 13.4, 4.3 Hz, 2H). Elemental Anal. C<sub>99</sub>H<sub>102</sub>YNa<sub>3</sub>O<sub>12</sub> Calc'd: C, 72.43%; H, 6.26%. Found: C, 71.15%; H, 6.15%.

[((R)-Sphenol)<sub>3</sub>YbNa<sub>3</sub>(thf)<sub>6</sub>]. Synthesized according to the general procedure, above, using 2.5 mg YbCl<sub>3</sub> (8.9  $\mu$ mol), 10 mg NaHMDS (55  $\mu$ mol, 6 equiv), and 9 mg (R)-sphenol (25  $\mu$ mol, 3 equiv) to afford 13 mg of the title compound as a light yellow solid (7.6  $\mu$ mol, 85%).

 $^{1}$ H NMR (400 MHz, CD<sub>3</sub>CN)  $\delta$  150.68, 42.86, 15.20, -8.61, -11.41, -16.04, -30.81. Elemental Anal. C<sub>99</sub>H<sub>102</sub>YbNa<sub>3</sub>O<sub>12</sub> Calc'd: C, 68.90%; H, 5.96%. Found: C, 69.07%; H, 6.01%.

[((S)-Sphenol)<sub>3</sub>YbNa<sub>3</sub>(thf)<sub>6</sub>]. Synthesized according to the general procedure, above, using 4.3 mg YbCl<sub>3</sub> (15  $\mu$ mol), 16 mg NaHMDS (87  $\mu$ mol, 6 equiv), and 16 mg (S)-sphenol (45  $\mu$ mol, 3 equiv) to afford 19 mg of the title compound as a light yellow solid (11  $\mu$ mol, 73%)

 $^{1}$ H NMR (400 MHz, CD<sub>3</sub>CN)  $\delta$  150.51, 42.72, 15.16, -8.56, -11.36, -15.94, and -30.66. Elemental Anal. C<sub>99</sub>H<sub>102</sub>YbNa<sub>3</sub>O<sub>12</sub> Calc'd: C, 68.90%; H, 5.96%. Found: C, 68.95%; H, 5.99%.

[((R)-Sphenol) $_3$ ErNa $_3$ (thf) $_6$ ]. Synthesized according to the general procedure, above, using 2.5 mg ErCl $_3$  (9.1  $\mu$ mol), 10 mg NaHMDS (55  $\mu$ mol, 6 equiv), and 9 mg (R)-sphenol (25  $\mu$ mol, 3 equiv) to afford 6 mg of the title compound as a pale pink solid (3.5  $\mu$ mol, 38%).

 $^{1}$ H NMR (400 MHz, CD<sub>3</sub>CN)  $\delta$  75.13, 22.17, -4.83, -19.44, -24.13, -31.48, -60.49. Elemental Anal. C<sub>99</sub>H<sub>102</sub>ErNa<sub>3</sub>O<sub>12</sub> Calc'd: C, 69.13%; H, 5.98%. Found: C, 68.91%; H, 5.99%.

[((5)-Sphenol)<sub>3</sub>ErNa<sub>3</sub>(thf)<sub>6</sub>]. Synthesized according to the general procedure, above, using 5 mg ErCl<sub>3</sub> (18  $\mu$ mol), 20 mg NaHMDS (109  $\mu$ mol, 6 equiv), and 19 mg (S)-sphenol (54  $\mu$ mol, 3 equiv) to afford 23 mg of the title compound as a pale pink solid (13  $\mu$ mol, 72%).

 $^{1}$ H NMR (400 MHz, CD<sub>3</sub>CN) δ: 74.86, 22.16, -4.84, -19.47, -24.14, -31.54, -60.58. Elemental Anal. C<sub>99</sub>H<sub>102</sub>ErNa<sub>3</sub>O<sub>12</sub> Calc'd: C, 69.13%; H, 5.98%. Found: C, 69.00%; H, 5.97%.

# ASSOCIATED CONTENT

# **Solution** Supporting Information

The Supporting Information is available free of charge at https://pubs.acs.org/doi/10.1021/acs.inorgchem.4c00417.

Supplemental spectra (UV-visible absorbance/excitation/emission, CPL, CD, NMR); computational details; tabulated photophysical measurements and further experimental details (PDF)

# AUTHOR INFORMATION

# **Corresponding Author**

Gaël Ung — Department of Chemistry, University of Connecticut, Storrs, Connecticut 06269, United States; orcid.org/0000-0002-6313-3658; Email: gael.ung@uconn.edu

# Author

David Schnable — Department of Chemistry, University of Connecticut, Storrs, Connecticut 06269, United States;
orcid.org/0000-0002-8650-997X

Complete contact information is available at: https://pubs.acs.org/10.1021/acs.inorgchem.4c00417

#### **Author Contributions**

All authors have given approval to the final version of the manuscript. D.S. conceptualized the work, performed the

synthesis and purification of the ligand and all metal complexes, collected NMR and optical spectra, designed/performed all DFT calculations and wrote the original draft of the manuscript. G.U. obtained elemental analysis, acquired funding, provided data validation and project supervision, and reviewed/edited the manuscript.

#### Notes

The authors declare no competing financial interest.

# ACKNOWLEDGMENTS

The authors would like to thank Nathan Schley for his efforts toward our attempts to crystallize these complexes, though unfortunately none of these were successful. The computational work performed in this project was done with help from the Storrs High-Performance Computing cluster. The authors would like to thank the UConn Storrs HPC and HPC team for providing the resources and support that contributed to these results. This material is based on work supported by the U.S. National Science Foundation under grant no. CHE-2041084.

# ABBREVIATIONS

CPL, circularly polarized luminescence; CD, circular dichroism; NIR, near-infrared; THF, tetrahydrofuran; HMDS, hexamethyldisilazide; DFT, density functional theory; CPCM, conductor-like polarizable continuum model; ZORA, zero-order regular approximation

#### REFERENCES

- (1) Farshchi, R.; Ramsteiner, M.; Herfort, J.; Tahraoui, A.; Grahn, H. T. Optical Communication of Spin Information between Light Emitting Diodes. *Appl. Phys. Lett.* **2011**, 98 (16), No. 162508.
- (2) Sherson, J. F.; Krauter, H.; Olsson, R. K.; Julsgaard, B.; Hammerer, K.; Cirac, I.; Polzik, E. S. Quantum Teleportation between Light and Matter. *Nature* **2006**, *443* (7111), 557–560.
- (3) MacKenzie, L. E.; Pal, R. Circularly Polarized Lanthanide Luminescence for Advanced Security Inks. *Nat. Rev. Chem.* **2021**, 5 (2), 109–124.
- (4) Stachelek, P.; MacKenzie, L.; Parker, D.; Pal, R. Circularly Polarised Luminescence Laser Scanning Confocal Microscopy to Study Live Cell Chiral Molecular Interactions. *Nat. Commun.* **2022**, 13 (1), No. 553, DOI: 10.1038/s41467-022-28220-z.
- (5) Schadt, M. Liquid Crystal Materials and Liquid Crystal Displays. *Annu. Rev. Mater. Sci.* **1997**, 27 (1), 305–379.
- (6) Baguenard, B.; Bensalah-Ledoux, A.; Guy, L.; Riobé, F.; Maury, O.; Guy, S. Theoretical and Experimental Analysis of Circularly Polarized Luminescence Spectrophotometers for Artifact-Free Measurements Using a Single CCD Camera. *Nat. Commun.* 2023, 14 (1), No. 1065
- (7) Sánchez-Carnerero, E. M.; Agarrabeitia, A. R.; Moreno, F.; Maroto, B. L.; Muller, G.; Ortiz, M. J.; de la Moya, S. Circularly Polarized Luminescence from Simple Organic Molecules. *Chem. Eur. J.* **2015**, *21* (39), 13488–13500.
- (8) Zinna, F.; Di Bari, L. Lanthanide Circularly Polarized Luminescence: Bases and Applications. *Chirality* **2015**, *27* (1), 1–13.
- (9) Carr, R.; Evans, N. H.; Parker, D. Lanthanide Complexes as Chiral Probes Exploiting Circularly Polarized Luminescence. *Chem. Soc. Rev.* **2012**, *41* (23), 7673–7686.
- (10) Muller, G. Luminescent Chiral Lanthanide(III) Complexes as Potential Molecular Probes. *Dalton Trans.* **2009**, 44, 9692–9707, DOI: 10.1039/b909430j.
- (11) Dhbaibi, K.; Favereau, L.; Crassous, J. Enantioenriched Helicenes and Helicenoids Containing Main-Group Elements (B, Si, N, P). *Chem. Rev.* **2019**, *119* (14), 8846–8953.
- (12) Lunkley, J. L.; Shirotani, D.; Yamanari, K.; Kaizaki, S.; Muller, G. Extraordinary Circularly Polarized Luminescence Activity Exhibited by Cesium Tetrakis(3-Heptafluoro-Butylryl-(+)-Camphorato)

- Eu(III) Complexes in EtOH and CHCl 3 Solutions. *J. Am. Chem. Soc.* **2008**, *130* (42), 13814–13815.
- (13) Riehl, J. P.; Richardson, F. S. Circularly Polarized Luminescence Spectroscopy. *Chem. Rev.* **1986**, 86, 1–16, DOI: 10.1021/cr00071a001.
- (14) Nagata, Y.; Mori, T. Irreverent Nature of Dissymmetry Factor and Quantum Yield in Circularly Polarized Luminescence of Small Organic Molecules. *Front. Chem.* **2020**, *8*, No. 448, DOI: 10.3389/fchem.2020.00448.
- (15) Arrico, L.; Di Bari, L.; Zinna, F. Quantifying the Overall Efficiency of Circularly Polarized Emitters. *Chem. Eur. J.* **2021**, 27 (9), 2920–2934.
- (16) Addanki, S.; Amiri, I. S.; Yupapin, P. Review of Optical Fibers-Introduction and Applications in Fiber Lasers. *Results Phys.* **2018**, *10*, 743–750.
- (17) Richardson, F. S. Selection Rules for Lanthanide Optical Activity. *Inorg. Chem.* **1980**, *19* (9), 2806–2812.
- (18) Bünzli, J.-C. Lanthanide Luminescence for Biomedical Analyses and Imaging. *Chem. Rev.* **2010**, *110* (5), 2729–2755.
- (19) Heffern, M. C.; Matosziuk, L. M.; Meade, T. J. Lanthanide Probes for Bioresponsive Imaging. *Chem. Rev.* **2014**, *114* (8), 4496–4539.
- (20) Amoroso, A. J.; Pope, S. J. A. Using Lanthanide Ions in Molecular Bioimaging. *Chem. Soc. Rev.* **2015**, *44* (14), 4723–4742.
- (21) Hemmer, E.; Venkatachalam, N.; Hyodo, H.; Hattori, A.; Ebina, Y.; Kishimoto, H.; Soga, K. Upconverting and NIR Emitting Rare Earth Based Nanostructures for NIR-Bioimaging. *Nanoscale* **2013**, 5 (23), 11339–11361, DOI: 10.1039/c3nr02286b.
- (22) Parker, D.; Fradgley, J. D.; Wong, K.-L. The Design of Responsive Luminescent Lanthanide Probes and Sensors. *Chem. Soc. Rev.* **2021**, *50* (14), 8193–8213.
- (23) Dhbaibi, K.; Grasser, M.; Douib, H.; Dorcet, V.; Cador, O.; Vanthuyne, N.; Riobé, F.; Maury, O.; Guy, S.; Bensalah-Ledoux, A.; Baguenard, B.; Rikken, G. L. J. A.; Train, C.; Le Guennic, B.; Atzori, M.; Pointillart, F.; Crassous, J. Multifunctional Helicene-Based Ytterbium Coordination Polymer Displaying Circularly Polarized Luminescence, Slow Magnetic Relaxation and Room Temperature Magneto-Chiral Dichroism\*\*. *Angew. Chem.* **2023**, *135* (5), No. e202215558.
- (24) Pointillart, F.; Lefeuvre, B.; Mattei, C. A.; Gonzalez, J. F.; Gendron, F.; Vincent, D.; Riobé, F.; Lalli, C.; Le Guennic, B.; Cador, O.; Maury, O.; Guy, S.; Bensalah-Ledoux, A.; Baguenard, B. Solid-State Near-Infrared Circularly Polarized Luminescence from Chiral YbIII-Single-Molecule Magnet. *Chem. Eur. J.* **2021**, *27*, 7362–7366, DOI: 10.1002/chem.202100903.
- (25) D'Aléo, A.; Picot, A.; Beeby, A.; Gareth Williams, J. A.; Le Guennic, B.; Andraud, C.; Maury, O. Efficient Sensitization of Europium, Ytterbium, and Neodymium Functionalized Tris-Dipicolinate Lanthanide Complexes through Tunable Charge-Transfer Excited States. *Inorg. Chem.* 2008, 47 (22), 10258–10268.
- (26) Willis, O. G.; Petri, F.; Pescitelli, G.; Pucci, A.; Cavalli, E.; Mandoli, A.; Zinna, F.; Di Bari, L. Efficient 1400–1600 Nm Circularly Polarized Luminescence from a Tuned Chiral Erbium Complex. *Angew. Chem., Int. Ed.* **2022**, *61* (34), No. e202208326.
- (27) Mukthar, N. F. M.; Schley, N. D.; Ung, G. Strong Circularly Polarized Luminescence at 1550 Nm from Enantiopure Molecular Erbium Complexes. J. Am. Chem. Soc. 2022, 144 (14), 6148–6153.
- (28) Adewuyi, J. A.; Schley, N. D.; Ung, G. Vanol-Supported Lanthanide Complexes for Strong Circularly Polarized Luminescence at 1550 nm. *Chem. Eur. J.* **2023**, 29 (36), No. e202300800.
- (29) Willis, O. G.; Pucci, A.; Cavalli, E.; Zinna, F.; Di Bari, L. Intense 1400–1600 Nm Circularly Polarised Luminescence from Homo- and Heteroleptic Chiral Erbium Complexes. *J. Mater. Chem. C* **2023**, *11* (16), 5290–5296.
- (30) Dee, C.; Zinna, F.; Kitzmann, W. R.; Pescitelli, G.; Heinze, K.; Di Bari, L.; Seitz, M. Strong Circularly Polarized Luminescence of an Octahedral Chromium(III) Complex. *Chem. Commun.* **2019**, *55* (87), 13078–13081.

- (31) Jiménez, J.-R.; Doistau, B.; Cruz, C. M.; Besnard, C.; Cuerva, J. M.; Campana, A. G.; Piguet, C. Chiral Molecular Ruby [Cr(Dqp)-2]3+ with Long-Lived Circularly Polarized Luminescence. *J. Am. Chem. Soc.* **2019**, *141* (33), 13244–13252.
- (32) Deng, M.; Schley, N. D.; Ung, G. High Circularly Polarized Luminescence Brightness from Analogues of Shibasaki's Lanthanide Complexes. *Chem. Commun.* **2020**, *56* (94), 14813–14816.
- (33) Willis, B.-A. N.; Schnable, D.; Schley, N. D.; Ung, G. Spinolate Lanthanide Complexes for High Circularly Polarized Luminescence Metrics in the Visible and Near-Infrared. *J. Am. Chem. Soc.* **2022**, *144* (49), 22421–22425.
- (34) Zhang, R.; Ge, S.; Sun, J. SPHENOL, A New Chiral Framework for Asymmetric Synthesis. *J. Am. Chem. Soc.* **2021**, *143* (32), 12445–12449.
- (35) Wang, L.; Yao, Z.; Huang, W.; Gao, T.; Yan, P.; Zhou, Y.; Li, H. Remarkable 980 Nm Circularly Polarized Luminescence from Dinuclear Yb(III) Helicates with a *D* 4 Symmetry. *Inorg. Chem. Front.* **2023**, *10* (12), 3664–3674.
- (36) Willis, O. G.; Zinna, F.; Pescitelli, G.; Micheletti, C.; Di Bari, L. Remarkable Near-Infrared Chiroptical Properties of Chiral Yb, Tm and Er Complexes. *Dalton Trans.* **2022**, *51*, 518–523.
- (37) Krylov, A. I. The Quantum Chemistry of Open-Shell Species. In *Reviews in Computational Chemistry*; Wiley, 2017; pp 151–224.
- (38) Grimme, S.; Antony, J.; Ehrlich, S.; Krieg, H. A Consistent and Accurate *Ab Initio* Parametrization of Density Functional Dispersion Correction (DFT-D) for the 94 Elements H-Pu. *J. Chem. Phys.* **2010**, 132 (15), No. 154104.
- (39) Goerigk, L.; Grimme, S. A Thorough Benchmark of Density Functional Methods for General Main Group Thermochemistry, Kinetics, and Noncovalent Interactions. *Phys. Chem. Chem. Phys.* **2011**, *13* (14), 6670–6688, DOI: 10.1039/c0cp02984j.
- (40) Pantazis, D. A.; Neese, F. All-Electron Scalar Relativistic Basis Sets for the Lanthanides. *J. Chem. Theory Comput.* **2009**, 5 (9), 2229–2238.
- (41) Pantazis, D. A.; Chen, X.-Y.; Landis, C. R.; Neese, F. All-Electron Scalar Relativistic Basis Sets for Third-Row Transition Metal Atoms. *J. Chem. Theory Comput.* **2008**, *4* (6), 908–919.
- (42) Weigend, F.; Ahlrichs, R. Balanced Basis Sets of Split Valence, Triple Zeta Valence and Quadruple Zeta Valence Quality for H to Rn: Design and Assessment of Accuracy. *Phys. Chem. Chem. Phys.* **2005**, 7 (18), 3297–3305, DOI: 10.1039/b508541a.
- (43) Tomasi, J.; Mennucci, B.; Cammi, R. Quantum Mechanical Continuum Solvation Models. Chem. Rev. 2005, 105 (8), 2999–3094.
- (44) D'Agostino, C.; Bräuer, P.; Charoen-Rajapark, P.; Crouch, M. D.; Gladden, L. F. Effect of Paramagnetic Species on T  $_1$ , T  $_2$  and T  $_1$  /T  $_2$  NMR Relaxation Times of Liquids in Porous CuSO  $_4$  /Al  $_2$  O  $_3$ . RSC Adv. 2017, 7 (57), 36163–36167.
- (45) Brachais, L.; Visseaux, M. NMR  $T_1$ -Relaxation Measurements on Paramagnetic Organolanthanides:An Alternative Tool for Structure Determination in Solution. *Eur. J. Inorg. Chem.* **2005**, 2005 (12), 2486–2492.
- (46) Ferenc, W.; Sadowski, P.; Cristóvão, B.; Sarzyński, J. Investigation of Some Physicochemical Properties of 4-Nitrocinnamates of Lanthanides(III). *J. Chil. Chem. Soc.* **2013**, *58*, 1753–1758, DOI: 10.4067/S0717-97072013000200025.
- (47) Van Vleck, J. H. The Theory of Electric and Magnetic Susceptibilities; Oxford University Press, 1965.
- (48) Parker, D.; Suturina, E. A.; Kuprov, I.; Chilton, N. F. How the Ligand Field in Lanthanide Coordination Complexes Determines Magnetic Susceptibility Anisotropy, Paramagnetic NMR Shift, and Relaxation Behavior. *Acc. Chem. Res.* **2020**, *53* (8), 1520–1534.
- (49) Bünzli, J.-C. G.; Eliseeva, S. V.Basics of Lanthanide Photophysics. In *Lanthanide Luminescence*; Springer, 2010; Vol. 7, pp 1–45.
- (50) Zatryb, G.; Klak, M. M. On the Choice of Proper Average Lifetime Formula for an Ensemble of Emitters Showing Non-Single Exponential Photoluminescence Decay. *J. Phys.: Condens. Matter* **2020**, 32 (41), No. 415902.